sustainability

MDPI

Article

Urban Heat Island Simulations in Guangzhou, China, Using the Coupled WRF/UCM Model with a Land Use Map Extracted from Remote Sensing Data

Guang Chen [1], Lihua Zhao [1,*] and Akashi Mochida [2]

[1] Building Environment and Energy Laboratory (BEEL), State Key Laboratory of Subtropical Building Science, South China University of Technology, Guangzhou 510641, China; chg401@163.com

[2] Department of Architecture and Building Science, Graduate School of Engineering, Tohoku University, Sendai 980-8579, Japan; mochida@sabine.pln.archi.tohoku.ac.jp

* Correspondence: lhzhao@scut.edu.cn; Tel.: +86-20-8711-2275

Academic Editors: Constantinos Cartalis and Matheos Santamouris
Received: 5 May 2016; Accepted: 30 June 2016; Published: 5 July 2016

Abstract: The Weather Research and Forecasting (WRF) model coupled with an Urban Canopy Model (UCM) was used for studying urban environmental issues. Because land use data employed in the WRF model do not agree with the current situation around Guangzhou, China, the performance of WRF/UCM with new land-use data extracted from Remote Sensing (RS) data was evaluated in early August 2012. Results from simulations reveal that experiments with the extracted data are capable of reasonable reproductions of the majority of the observed temporal characteristics of the 2-m temperature, and can capture the characteristics of Urban Heat Island (UHI). The "UCM_12" simulation, which employed the extracted land-use data with the WRF/UCM model, provided the best reproduction of the 2-m temperature data evolution and the smallest minimum absolute average error when compared with the other two experiments without coupled UCM. The contributions of various factors to the UHI effect were analyzed by comparing the energy equilibrium processes of "UCM_12" in urban and suburban areas. Analysis revealed that energy equilibrium processes with new land use data can explain the diurnal character of the UHI intensity variation. Furthermore, land use data extracted from RS can be used to simulate the UHI.

Keywords: WRF/UCM model; remote sensing; numerical simulation; urban heat island

1. Introduction

Urbanization is a population shift from rural to urban areas, and also covers the ways in which society adapts to this change. It predominantly results in land use and land cover changes and increased building density, both horizontally and vertically, in urban areas. Land use and land cover changes associated with urbanization can have a considerable impact on urban climate [1]. One phenomenon is a consistent rise in temperature in the urban atmosphere caused by the land use changes, and the accompanying effects on the physical processes governing energy, momentum, and matter exchanges between the land surface and the atmosphere [2,3]. Guangzhou, the capital and largest city of Guangdong Province and the third largest city in China, is undergoing rapid and widespread urbanization and a deterioration of the urban environment caused by Urban Heat Island (UHI).

The Weather Research and Forecasting (WRF) model, coupled with an Urban Canopy Model (UCM), was developed as a community tool for studying urban environmental issues [4,5]. The coupled WRF/UCM modeling system has been applied to many regions, such as Houston, USA [6], Nanjing, China [7], and New York, USA [8], and its performance has been evaluated against observations.

Many studies have performed simulations using land use data from different years with the single-layer urban canopy model in the Noah land surface model to demonstrate that urban development and the accompanying land use changes can make a significant contribution to extreme heat events [9–12]. However, the default data (U.S. Geological Survey (USGS) land use) employed in the WRF model are based on the NationalOceanic and Atmospheric Administration (NOAA) 1-km Advanced Very High Resolution Radiometer (AVHRR) data obtained from 1992 to 1993. Owing to the rapid urban expansion in the past decade in China, the USGS data are considered outdated. Numerical simulations in Guangzhou [9] and Chengdu [13] with the new land use data reproduced better 2-m temperature evolution data with a smaller minimum absolute average error compared with results obtained using the default USGS land use data in the WRF model. Versions of the WRF model after version 3.1 provide an alternative land use dataset based on the Moderate Resolution Imaging Spectroradiometer (MODIS) 2001 satellite products. Implementation of MODIS data results in better performance of the coupled WRF/UCM modeling system, although the urban area in MODIS also falls short of reality because of fast urbanization [14]. The diurnal variations of UHI intensity and the spatial distribution of the UHI effect in Beijing have been reproduced well by the WRF/UCM with MODIS data [15]. The simulation results with MODIS data improved predictions of the accumulated rainfall when compared with the simulation performed using USGS data [16]. Numerical simulations of Taiwan showed that results obtained using MODIS land use data are in better agreement with the observed data than those obtained using USGS data, although MODIS land use data overestimated the urban area [17]. When compared with observational data, numerical simulations in Guangzhou [18] showed improved accuracy using MODIS data compared with USGS data, but poorer accuracy than that obtained using land use data extracted from the Landsat-7 remote sensing dataset. The effect of urbanization on the weather and climate in Hangzhou were investigated using the coupled WRF/UCM model with updated land use data, and the research showed that updated land use data can reproduce the local climate accurately, and that urban land use has a significant impact on the simulated UHI effect [19].

In this study, the land-use data were extracted from the remote sensing dataset of Landsat-7 using a previous research [20] method and then up-to-date extracted land-use data classified as urban land cover were divided into three urban subcategories by satellite-measured night time light data and the normalized difference vegetation index dataset. The mesoscale coupled WRF/UCM model with different land-use data are used to simulate the formation of high-temperature synoptic conditions in the area of Guangzhou in early August 2012. The aim of this research is to demonstrate that, when using the extracted and up-to-date urban land use data from a remote sensing dataset, the WRF/UCM modeling system provides a more accurate simulation of urban temperatures and the UHI effect in Guangzhou. Furthermore, the study aims to simulate the formation of high-temperature synoptic conditions in the area of Guangzhou, and to investigate the properties of coupled WRF/UCM model and their effects on the UHI simulations.

2. Data Sources and Methodology

2.1. Study Area

The study area is located in Guangzhou, south China, with a population of 12.78 million as of the 2010 census. Located in the south-central portion of Guangdong, Guangzhou spans between 112°57′ and 114°03′E longitudes, and 22°26′ and 23°56′N latitudes. Located just south of the Tropic of Cancer, Guangzhou has a humid subtropical climate that is influenced by the East Asian monsoon. Summers are wet with high temperatures, and high heat index. The hottest period in summer usually lasts from 11 July to 20 August, with an average period of 41 days. The mean annual temperature in the city is 22.3 °C, with monthly daily averages ranging from 12.3 °C in January to 28.4 °C in July.

Guangzhou is expanding at a very high speed. Statistical data from the China City Statistical Yearbook show that the built-up area in Guangzhou city has increased more than 4 times since the year 2000, which is much faster than the average expansion pace in China. Such tremendous urban

expansion accompanied with increasing built-up areas and intensifying human activities causes remarkable modifications of the underlying surface properties, thereby significantly enhancing the UHI effect [17]. Previous studies show that the UHI effect noticeably contributes to regional warming in Guangzhou area [21]. This study area includes the seven main districts of Guangzhou, all of which are undergoing rapid urban expansion.

2.2. Model Configuration

The WRF version 3.2 model, coupled with a sophisticated single-layer UCM, was used in this study [5]. Three one-way nested domains with 72 × 72, 101 × 101, and 121 × 121 grid points, and grid spacings of 25, 5, and 1 km, respectively, were used (Figure 1). The coordinate of the domain's center is 22°6′57″N by 113°31′8″E. The largest domain (Domain 1) covers most of southern China and the second domain covers the whole Guangdong area. The main districts of Guangzhou are covered by Domain 3. The integration starts at 0:00 GMT on 20 July 2012 for a period of one month. Four days from 1 August to 4 August were selected to evaluate performance of the WRF/UCM with different land-use data.

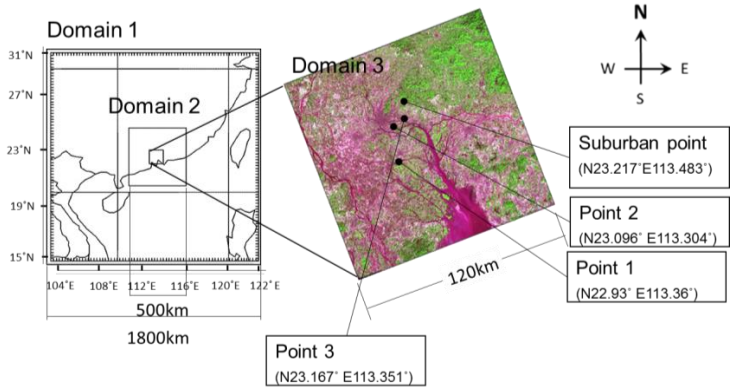

Figure 1. The three nested domains used for the numerical simulation and the location of comparison points.

The parameterization schemes used in our simulation are listed in Table 1, including long- and short-wave radiation processes, planetary boundary layer processes, land surface processes, microphysical processes, etc. In the WRF model, a single-layer UCM was implemented in the NOAH land surface model to account for the thermal and dynamic effects of urban buildings, including the trapping of radiation within the urban canopy. The UCM standard values for heat capacity, conductivity, albedo, and emissivity roughness length for heat and momentum of roof, road, and wall surfaces were employed [4,22]. Initial and lateral boundary conditions were taken from the National Centers for Environmental Prediction (NCEP) Global Forecast System Final Analyses (horizontal resolution of 1° × 1°) with 6-h intervals.

Table 1. WRF configurations.

Simulation Time	**20 July 2012 00:00–20 August 2012 00:00 (GMT)**
Meteorological data	National Centers for Environmental Prediction Final Operational Global Analysis data
Long-wave radiation	Rapid radiative transfer model (RRTM) long-wave radiation scheme
Short-wave radiation	Dudhia short-wave radiation scheme
Surface layer	Monin–Obukhov scheme
Land surface	Noah land-surface model+ single-layer Urban Canopy Model (UCM)
Cumulus	Kain–Fritsch (new Eta) scheme
Short-wave radiation	Dudhia scheme
Micro-physics	WRF Double-Moment 6-class
Boundary layer	Yonsei University (YSU) boundary layer scheme

2.3. Updated Land Use Data

To derive and classify each land use class from the Landsat-7 ETM+ images, a supervised classification with the maximum likelihood method, which is the same method as the previous research [20], was only applied to the Domain 3. Supervised classification is a procedure most often used for quantitative analysis of remote sensing image data. It is based on using suitable algorithms to label the pixels in an image as representing particular ground cover classes [23]. The extracted land use classes are essentially consistent with the ones defined from MODIS land use classes of forest, grassland, wetland, cropland, urban, barren land, and water. These land use data are almost the same as the previous research result, here named RS_12 [20]. There is only one urban land category in RS_12 and thus these data cannot reproduce urban effects on local climate caused by heterogeneity in an urban area. A human settlement index (HSI) [24], based on satellite-measured nighttime light imagery and the normalized difference vegetation index (NDVI), was used to divide the extracted urban land cover into three urban subcategories: commercial/industrial/transportation (CIT), high-intensity residential (HIR), and low-intensity residential (LIR).

HSI data were obtained from a combination of nighttime light imagery and the normalized difference vegetation index (NDVI) [24], as expressed in Equation (1).

$$\mathrm{HSI} = \frac{(1 - \mathrm{NDVI_{max}}) + \mathrm{OLS_{nor}}}{1 - \mathrm{OLS_{nor}} + \mathrm{NDVI_{max}} + \mathrm{NDVI_{max}} \times \mathrm{OLS_{nor}}} \quad (1)$$

where OLS_{nor} is the normalized value of the 2012 Defense Meteorological Satellite Program/Operational Linescan System (DMSP/OLS) image [25,26], expressed by Equation (2). A threshold of 23 was selected to minimize the effects of blooming, a phenomenon observed in DMSP/OLS nighttime imagery. OLS_{max} is the maximum value in the 2012 DMSP/OLS nighttime light image.

$$OLS_{\mathrm{nor}} = \frac{(\mathrm{OLS} - 23)}{(OLS_{\mathrm{max}} - 23)} \quad (2)$$

To separate human settlements from bare land effectively, and to remove the effect of cloud contamination, 2012 multi-temporal SPOT NDVI images at a resolution of 1 km × 1 km were used to generate a new NDVI composite index, as shown in Equation (3) [27].

$$NDVI_{\mathrm{max}} = \mathrm{MAX}\,(\mathrm{NDVI1}, \mathrm{NDVI2}, \ldots, \mathrm{NDVI23}) \quad (3)$$

HSI values were used to classify urban land in Guangzhou into the following subcategories: (1) pixels with HSI values ⩾80th percentile, represented as CIT areas; (2) pixels with HSI values between the 30th and the 80th percentiles, represented as HIR areas; and (3) pixels with HSI values ⩽30th percentile, represented as LIR areas. The extracted urban land use data were classified into the three urban land cover categories to represent up-to-date urbanization conditions in Guangzhou. These Landsat-7 extracted and then enhanced land use data, named UCM_12, are shown in Figure 2a and the default Modis land use data are shown in Figure 2b. The area in Figure 2 indicates the square in Domain 3.

2.4. Numerical Experiments

To understand how well the WRF/UCM simulates the UHI effect in urban environments, three numerical experiments were designed to run with or without the UCM model, and using either the MODIS data or the extracted land use data (Table 2). Sensitivity experiments were conducted as follows: (1) MODIS experiment, integrated solely by the WRF model not coupled with UCM and based on the MODIS land use data, the detailed land use map is shown in Figure 2b; (2) RS_12 experiment, also integrated without UCM and based on the Landsat-7 extracted land use data for 2012; and (3) an experiment based on the enhancement of the extracted land use data from Landsat-7 with HSI and coupled with the UCM model. The physics schemes remained the same for all runs.

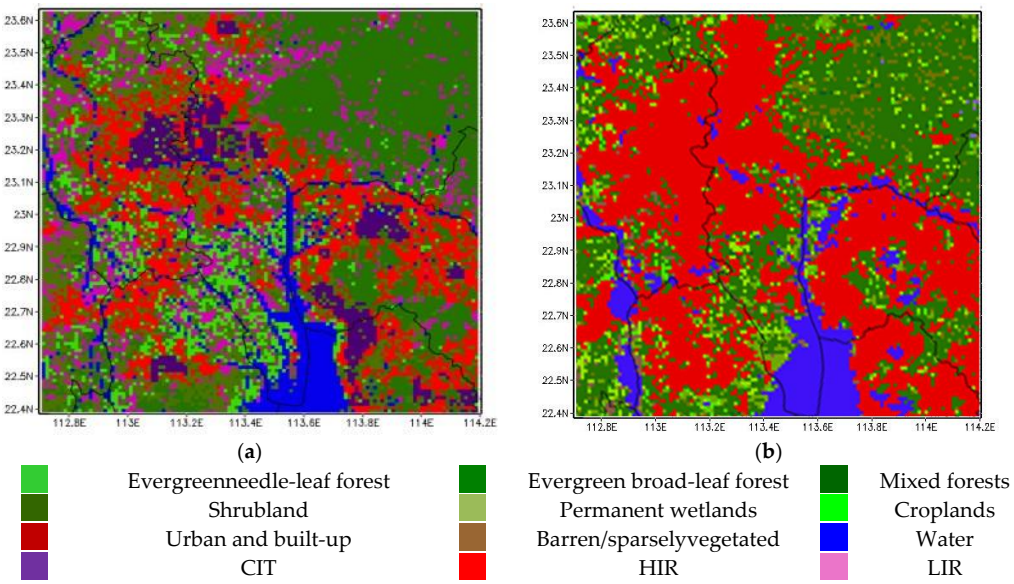

Figure 2. Types of land use data in Domain 3: (**a**) UCM_12, enhancement of the extracted land use data from Landsat-7 with HIS; and (**b**) Modis, default land use data in WRF.

Table 2. Experiment design.

Experiments	UCM	Land Use
Modis	No	MODIS
RS_12	No	Extracted from Landsat-7 RS data
UCM_12	Yes	Enhancement of the extracted land use data from Landsat-7 by HSI

2.5. Observational Data

The simulation lasts for one month, as obtaining long time data to evaluate performance of the WRF/UCM and the land use data is better. Only four days of climate data from 1 August 0:00 (GMT) to 4 August 24:00 (GMT) 2012 were acquired from the Guangzhou Meteorological Bureau. The first two days were sunny and high-temperature weather, whereas rainy and cloudy weather was observed on the last two days. The observational data were gathered from four weather stations (one in a suburban area, and three in urban areas) in Domain 3. The suburban weather station (suburban point in Figure 1) is located on an elevation in the mountainous and hilly terrain far away from the downtown of Guangzhou, such that there are no tall buildings and medium-sized enterprises within 3 km, and the station is not shaded. The other three weather stations (Points 1–3 in Figure 1) are located in the urban area. The area around Point 1 experiences rapid urbanization, and thus its representation greatly differs between the MODIS and extracted land use map. Points 2 and 3 are located in the old down town. Points 1 and 2 were representative points for the model evaluation. Hourly temperature and wind velocity data were collected to investigate the UHI characteristics and the performance of the WRF/UCM model with the extracted land use data.

3. Simulation Analysis

3.1. Air Temperature at 2-m Height

To investigate the performance of the WRF/UCM model with the extracted land use data, we compared the results of the three experiments with the 2-m temperature data observed at the automatic weather stations. Figure 3a presents the observed and modeled air temperature at 2-m height lasting 20 days from 20 July to 9 August in the suburban area, and the four-day comparison from 1 August to 4 August was analyzed in the urban areas (Figure 3b).

From Figure 3a, it can be found that the modeled daily temperature cycles are generally consistent with the observational data on sunny and hot days, but vary in magnitude on rainy days. The same characteristic can be found in Figure 3b: all models performed better on 1 and 2 August than on 3 and 4 August because of the rainy and cloudy weather seen on the latter two days. All of the experimental schemes showed the diurnal variation of temperature in urban and suburban areas, though with varying magnitudes. The air temperature from the MODIS experiment was lower than the observed data during the period 0:00–12:00 at the suburban station, but the RS_12 and UCM_12 experiments gave lower temperatures from 06:00–12:00. In Figure 3b, all the modeled air temperatures were higher than the observed data, and there was a good fit for the maximum air temperature between the three experiments and the observed data for 1 and 2 August.

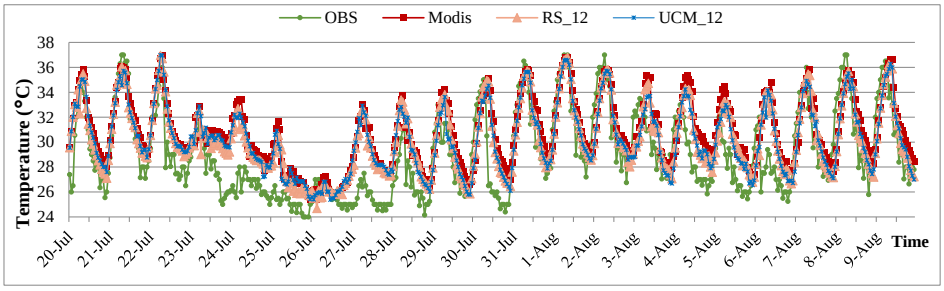

(**a**)

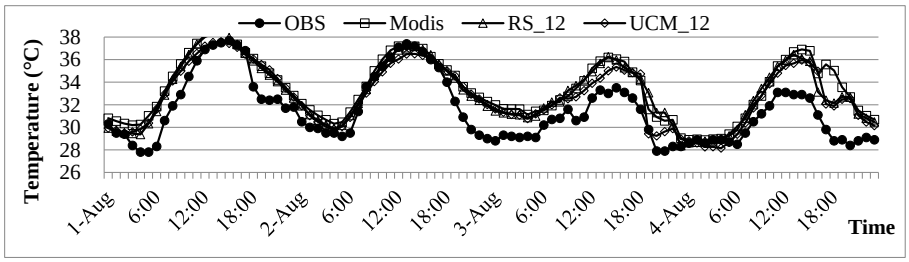

(**b**)

Figure 3. Comparison of the air temperature at 2-m height simulated in the three experiments with the observed temperature (OBS): (**a**) Suburban station; and (**b**) Point 1.

The simulated and observed daily mean (T2M), maximum (T2MAX), and minimum (T2MIN) 2-m air temperatures are shown in Table 3. In general, the UCM_12 experiment efficiently simulated the daily variations in near-surface air temperature, and the RS_12 results were better than the MODIS on the near-surface air temperature simulation results.

Table 3. Comparison of the simulated and observed 2-m temperatures (T2).

	Suburban				Urban *			
	OBS	**MODIS**	**RS_12**	**UCM_12**	**OBS**	**MODIS**	**RS_12**	**UCM_12**
T2M (°C)	30.4	31.8	31.3	31.2	32.8	34.3	33.6	33.4
T2MAX (°C)	37.0	36.8	36.8	36.6	37.5	38.1	37.8	37.3
T2MIN (°C)	26.6	27.9	27.1	26.7	28.0	30.2	29.0	28.9

*: The average results over 3 urban points.

Willmott suggested using the root mean square error ($RMSE$), systematic ($RMSE_S$) and unsystematic ($RMSE_U$) errors, and an index of agreement d to evaluate the simulation performance [28]. The index of agreement d can be interpreted as a measure of how error-free a model predicts a variable. The RMSE summarizes the magnitude of the average difference between observation and prediction.

Systematic errors, described by $RMSE_S$, result from causes which occur consistently. $RMSE_U$ gives information about unsystematic errors, which consist of a number of small effects are positive and some are negative in terms of affecting the final output value. The good model therefore has a systematic difference of zero while the unsystematic difference should approach the $RMSE$. The d value of 1.0 indicates perfect agreement between observation and prediction. The d can be calculated by Equation (4) [28,29].

$$d = 1 - \frac{\sum_{i=1}^{N} (P_i - O_i)^2}{\sum_{i=1}^{N} \left(|P_i'| + |O_i'|\right)^2}, (0 \leqslant \mathrm{d} \leqslant 1) \quad (4)$$

where $P_i' = P_i - \overline{O}$, $O_i' = O_i - \overline{O}$. $\overline{O}$ is the average of the observational data.

The index of agreement d describes how accurately a model predicts a variable. When d value is equal to 1.0, it indicates perfect prediction for the variable.

The difference measures for the four comparison points 2-m temperature are summarized in Table 4. The RMSE for the three simulations at the four weather stations ranged from 1.41 to 2.86 °C. Additionally, the systematic errors ($RMSE_S$) were comparatively small and the unsystematic errors ($RMSE_U$) approached the RMSE in UCM_12, indicating that the UCM_12 experiment fits the criteria of the systematic error. The d values for all of the simulations at the four stations ranged from 0.74 to 0.95, suggesting that all three experiments provided a reasonable approximation of the observed data. Comparing the d values for the three simulations for each point, the value at UCM_12 is highest, followed by the RS_12 d value, which is in turn larger than the MODIS d value. This suggests that the extracted land use data used in WRF/UCM model provide the best reproduction of temperature variations among the three simulations in both suburban and urban areas. Additionally, the results show that the extracted land use data provided a better simulation than the MODIS data.

Table 4. Quantitative evaluation of three cases' performance on temperature compared with observed data.

Comparison Points	MODIS			
	d	**RMSEs**	**RMSEu**	**RMSE**
Suburban point	0.79	1.48	1.88	2.40
Point 1	0.82	2.00	1.42	2.45
Point 2	0.88	0.60	1.47	1.59
Point 3	0.74	2.37	1.60	2.86
	RS_12			
	d	**RMSEs**	**RMSEu**	**RMSE**
Suburban point	0.86	1.03	1.72	2.00
Point 1	0.86	1.70	1.33	2.15
Point 2	0.90	0.34	1.37	1.41
Point 3	0.94	2.26	1.45	2.69
	UCM_12			
	d	**RMSEs**	**RMSEu**	**RMSE**
Suburban point	0.89	1.03	1.73	2.01
Point 1	0.90	1.46	1.38	2.02
Point 2	0.93	0.29	1.51	1.53
Point 3	0.95	2.10	1.69	2.69

3.2. Urban Heat Island Intensity (UHII)

By comparing the results of the three numerical experiments, their ability to simulate the urban heat island effect can be examined. Figure 4 presents the evolution of the urban heat island intensity (UHII) as simulated by the three experiments. The intensity of the heat island is calculated as the difference of temperature between urban Point 1 and the suburban point at 2-m height. As shown

by the observations, the UHII gradually increases after midday, reaching a maximum at night, with a maximum temperature difference of more than 5 °C. The UHII then gradually decreases in the morning, even becoming negative at noon.

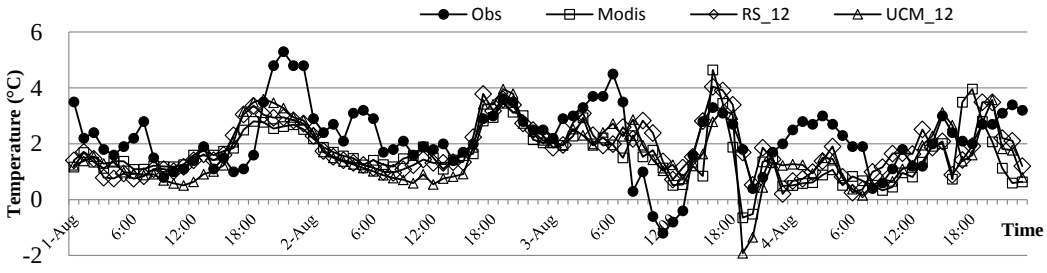

Figure 4. Heat island intensity of the different experiments at Point 1.

All experiments plausibly reproduce the characteristics of UHII evolution, except for on 3 August, when the negative UHII is weakly reproduced and its overall variation is underestimated. UCM_12 produces a better reproduction of the UHII at peak values, but a poorer reproduction than the other experiments at other times.

The maximum UHII and the average local UHII reflect the average difference over the whole day, and were selected to analyze the UHI effect.

Modeled and observed values of maximum UHII at Point 1 and Point 2 are compared in Figure 5a,b, respectively. At Point 1, the RS_12 and UCM_12 results have better correspondence to the observations than the MODIS results. The UCM_12 experiment did not show a noticeably better performance among the simulations despite the implementation of the coupled WRF/UCM model. At Point 2, although the UCM_12 experiment showed a higher maximum UHII, there is still a large deviation from the observations. On 3 August, none of the experiments agreed with the observations, predominantly because of the rainy weather.

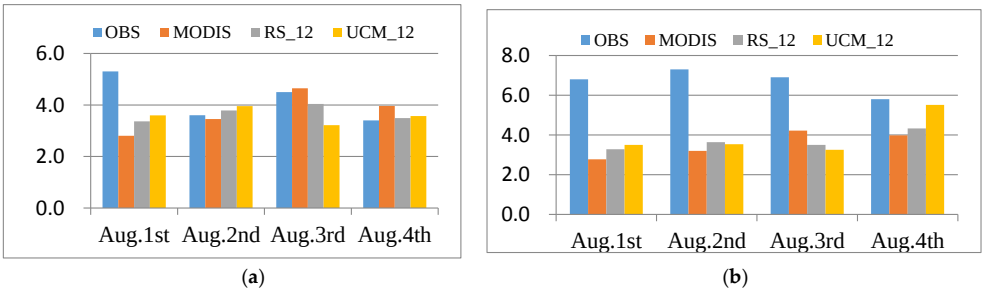

Figure 5. The Maximum UHII: (**a**) Point 1; and (**b**) Point 2.

The average local UHII were calculate by Equation (5),

$$UHII_{\text{avg}} = \frac{\int_{t0}^{t1} T_u dt - \int_{t0}^{t1} T_r dt}{\int_{t0}^{t1} dt} \quad (5)$$

where, T_u stands for the hourly 2-m height temperature in the urban area, T_r stands for the hourly 2-m height temperature in the suburban area, t_0 stands for initial time of the simulation, and t_1 stands for end time of the simulation.

The average local UHII for all experiments and the observation data at Point 1 and Point 2 are shown in Figure 6a,b. The daytime was constrained between 8:00 and 20:00 and the rest was considered as nighttime. All experiments have a better agreement with the observations and represent larger magnitudes of average local UHII at Point 2 than at Point 1. All experiments underestimate both

day- and nighttime UHII. In urban areas, the UCM_12 experiment produces poor statistical scores for the average daytime local UHII, but better ones for the average nighttime local UHII. The UCM_12 experiment produces the highest average nighttime local UHII, although the value is still lower than the observed one.

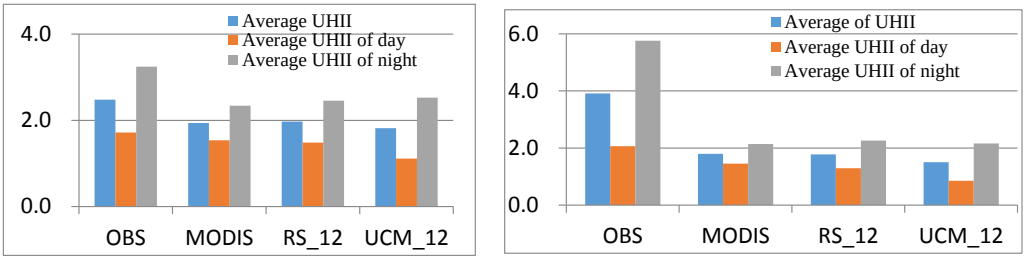

(**a**) (**b**)

Figure 6. The average local UHII: (**a**) Point 1; and (**b**) Point 2.

Although the results of the coupled WRF/UCM model do not accurately reproduce the observations and reveal consistently underestimated UHII, they feasibly reflect the diurnal variation of the UHII. Additionally, the coupled WRF/UCM model exhibits better performance with the extracted land use data than with the MODIS land use data.

3.3. Wind Velocity at 10-m Height

Regarding wind velocity, all of the simulation results were close to the observation data in the daytime. The observed and simulated wind velocity at 10-m height at the suburban point and Point 1 are shown in Figure 7a,b, respectively. In general, wind velocity simulated in all three experiments is overestimated, and the distribution trends of all the experiments are similar when comparing the simulations and observations. For the urban area, both modeled and observed wind velocity is lower in the nighttime, which corresponds to the changes in UHI intensity. It is believed that the strong thermal stability of the surface layer is the primary reason for nighttime enhancement of UHI. It should also be noted that surface wind speed is generally reduced in a stable surface layer. All experiments have large magnitudes compared with the observations. Even using the coupled WRF/UCM model, the influence of the buildings on the wind environment cannot be reproduced.

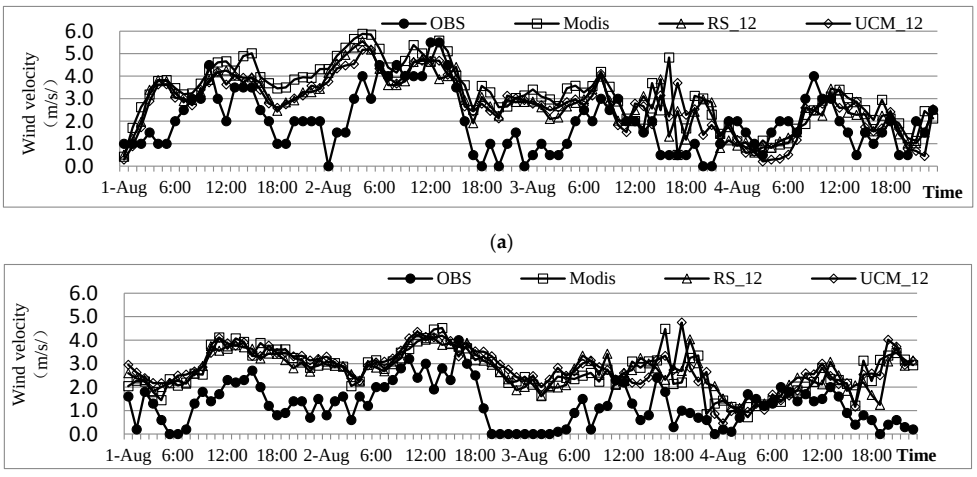

(**a**)

(**b**)

Figure 7. Comparison of the wind velocity at 10-m height simulated in the three experiments with observations: (**a**) Suburban station; and (**b**) Point 1.

The difference measures of the modeled wind velocity at 10-m height of four comparison points are summarized in Table 5. The *d* values for all experiments at the four stations ranged from 0.34 to 0.70, indicating low consistency of simulations with the observed data. At the same time, the systematic errors ($RMSE_S$) were comparatively small and the unsystematic errors ($RMSE_U$) approached the RMSE in UCM_12, indicating better performance of coupled WRF/UCM with extracted land use data compared to other cases, although the improvement is relatively small.

Table 5. Quantitative evaluation of three cases' performance on wind velocity compared with observed data.

Comparison Points	MODIS			
	d	**RMSEs**	**RMSEu**	**RMSE**
Suburban point	0.64	1.59	1.31	2.06
Point 1	0.51	1.54	0.78	1.73
Point 2	0.44	1.42	0.74	1.61
Point 3	0.43	1.59	0.82	1.79
	RS_12			
	d	**RMSEs**	**RMSEu**	**RMSE**
Suburban point	0.68	1.03	1.72	2.00
Point 1	0.49	1.65	0.77	1.82
Point 2	0.34	2.10	0.85	2.27
Point 3	0.53	1.24	1.45	2.69
	UCM_12			
	d	**RMSEs**	**RMSEu**	**RMSE**
Suburban point	0.70	1.01	1.01	1.47
Point 1	0.52	1.55	0.64	1.68
Point 2	0.45	1.42	0.74	1.61
Point 3	0.50	1.35	0.80	1.57

3.4. Energy Balance Data

The UHI is mainly determined by the surface energy balance [30], and the contributing factors during land surface energy equilibrium processes on the UHI can be represented in models. To focus on the formation of the UHI on 1 August and to investigate the performance of the UCM in simulating the UHI, the energy equilibrium processes between urban and suburban areas, and between experiments UCM_12 and RS_12, were compared and analyzed. Figure 8 shows the temporal variability of parameters relevant to the land surface energy equilibrium in the urban area during the UCM_12 experiment from 1 August 00:00 (GMT) to 23:00 (GMT).

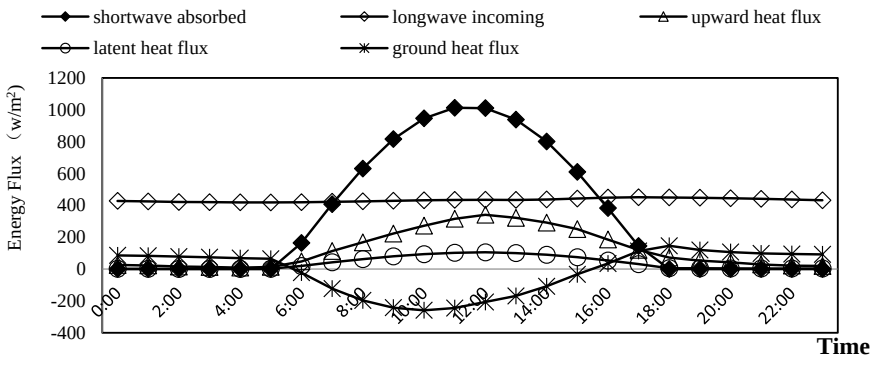

Figure 8. Temporal evolution of parameters relevant to the land surface energy equilibrium in the urban area during the UCM_12 experiment on 1 August.

The absorption of solar short-wave radiation is predominantly an energy input, whereas the outputs are latent heat flux and ground heat flux. Long-wave radiation shows weak daily variation (approximately 450 W/m^2). Ground heat flux and upward heat flux reach their maximum values of 250 and 340 W/m^2, respectively, in the daytime around noon. The latent heat flux only reaches a maximum of 100 W/m^2 owing to evaporation, which is absent at night. At night, the ground heat flux acts as an input, becoming a major source of energy, while the upward heat flux, though much smaller than during the daytime, remains positive as it continues to transfer heat to the atmosphere. The characteristics of these energy equilibrium processes suggest a positive performance when simulating the UHI using the WRF/UCM with the land use data extracted from remote sensing data.

Figure 9 presents the differences in the energy equilibrium between Point 1 and the suburban point simulated in the UCM_12 experiment. Urban areas absorb more short-wave radiation than suburban areas, although the difference is small. The diurnal latent heat flux was significantly different between the urban and suburban areas. During the day, the latent heat flux was reduced in urban areas because of the limited vegetation and less evaporation, while it remained small at night. During the day, the upward heat flux was significantly higher in the urban area than in the suburban areas, close to 200 W/m^2. After sunset, the difference in the ground heat flux turns from negative to positive, while that of upward heat flux remained positive. The positive heat fluxes, though small, resulted in a higher temperature at night in urban areas than in suburban areas. The WRF model simulation of UHI with the land use data extracted from remote sensing data can reveal the causes of the UHI.

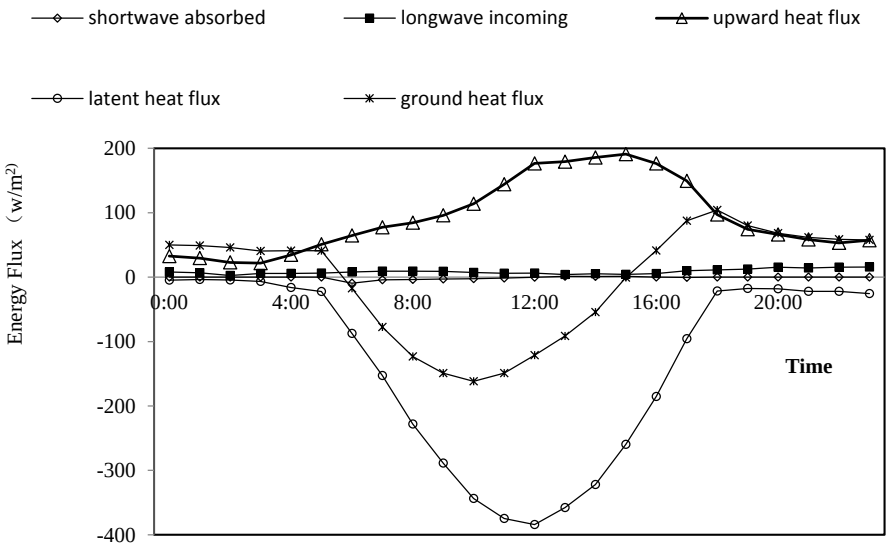

Figure 9. Differences in the energy equilibrium between Point 1 and the suburban point for the UCM_12 simulation.

Figure 10 shows the differences between the individual terms of energy equilibrium between the UCM_12 and RS_12 experiments. The improvement of the simulation performance by the UCM model can be illustrated from the difference. The urban latent heat flux is reduced in the daytime when coupled UCM the model in UCM_12, the reduction reaches a maximum of 100 W/m^2. In addition, the UCM_12 simulation suggested a larger diurnally upward heat flux and ground heat flux than the RS_12 simulation. This suggests that the urban canopy model can be used to improve nighttime UHI simulations.

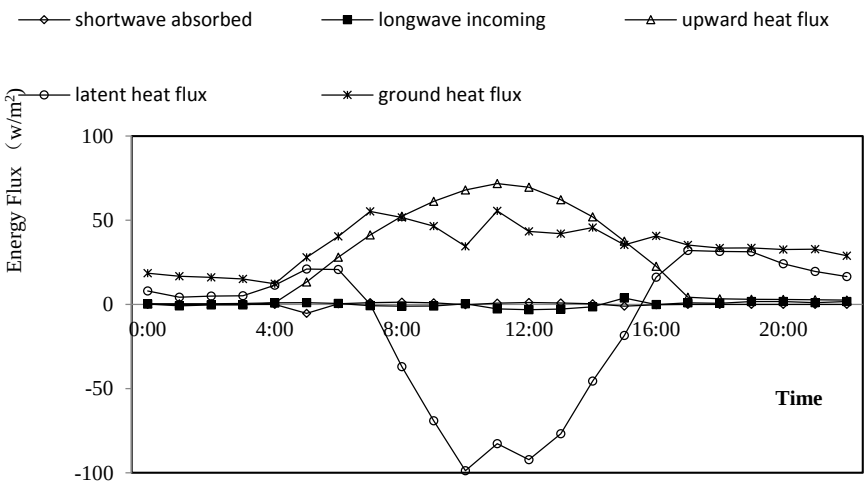

Figure 10. Differences in the energy equilibrium between the UCM_12 and RS_12 simulation.

4. Summary and Conclusions

The thermal environment over Guangzhou from late July to early August 2012 was investigated using the coupled WRF/UCM model. Simulation experiments were performed using both the urban land use data extracted from remote sensing datasets and the default MODIS data.

(1) Using the new land use data, the simulated 20 days of daily temperature cycles at the suburban weather station and four days of daily temperature cycles at urban point showed an encouraging agreement with observations, especially on hot sunny days. UCM_12 simulated maximum diurnal temperatures closer to the observed values than the simulations that excluded the UCM model. The coupled WRF/UCM with the new land use data improved the simulation performance.

(2) Compared with the maximum UHII and the average local UHII, all of the simulated results reproduced the diurnal characteristics of UHI intensity. Both RS_12 and UCM_12 simulations performed better than the default geographic model, although they did not perfectly replicate the observations.

(3) The modeled wind velocity results were higher than observations. The new land use data produced similar results as the default land use data. For the urban area, all wind velocity simulation results and observations were lower, and the UHII remains high during the nighttime.

(4) The UCM_12 experiment successfully reproduced the differences in the energy equilibrium both in the urban and suburban areas. In the urban area, most of the input energy is used in sensible heating, which resulting the higher temperature, can be simulated by the WRF/UCM. The latent heat flux in the urban area is lower than in suburban area because lack of evapotranspiration of water vapor in the urban area. For the nocturnal situation, relatively high minimum temperature is reproduced in the urban owing to the sustained upward ground heat flux heats the atmosphere in the urban area.

As changing the land use data can have a significant impact on the WRF/UCM simulation result, this study confirmed that the WRF/UCM model with land use data extracted from a remote sensing dataset can be an effective tool for urban thermal environment analyses.

Acknowledgments: This study was supported by the State Key Laboratory of Subtropical Building Science, South China University of Technology, China (Project No. 2015ZC12); the National Natural Science Foundation of China (Project No. 51408303); and the China Scholarship Council Program (No. [2013]3009). Helpful comments from Yufeng Zhang and Xiaoshan Yang were greatly appreciated.

Author Contributions: All three authors significantly contributed to the scientific study and writing. Guang Chen and Lihua Zhao contributed to the overall idea, planning, financing, analyzing and writing of the manuscript, and

conceived and designed the simulation. Akashi Mochida contributed to discussions on the land use data issues of this paper and manuscript preparations.

Conflicts of Interest: The authors declare no conflict of interest.

Abbreviations

The following abbreviations are used in this manuscript:

WRF	Weather Research and Forecasting
UCM	Urban Canopy Model
UHI	Urban Heat Island
CIT	Commercial/Industrial/Transportation
HIR	High-Intensity Residential
LIR	Low-Intensity Residential
UHII	Urban Heat Island Intensity

References

1. Foley, J.A.; DeFries, R.; Asner, G.P.; Barford, C.; Bonan, G.; Carpenter, S.R.; Chapin, F.S.; Coe, M.T.; Daily, G.C.; Gibbs, H.K.; et al. Global consequences of land use. *Science* **2005**, *309*, 570–574. [CrossRef] [PubMed]
2. Cotton, W.R.; Pielke, R.A. *Human Impacts on Weather and Climate*; Cambridge University Press: Cambridge, UK, 2007.
3. Zhang, C.L.; Chen, F.; Miao, S.G.; Li, Q.C.; Xia, X.A.; Xuan, C.Y. Impacts of urban expansion and future green planting on summer precipitation in the Beijing metropolitan area. *J. Geophys. Res. Atmos. (1984–2012)* **2009**. [CrossRef]
4. Kusaka, H.; Kondo, H.; Kikegawa, Y.; Kimura, F. A simple single-layer urban canopy model for atmospheric models: Comparison with multi-layer and slab models. *Bound.-Layer Meteorol.* **2001**, *101*, 329–358. [CrossRef]
5. Chen, F.; Kusaka, H.; Bornstein, R.; Ching, J.; Grimmond, C.S.B.; Grossman-Clarke, S.; Loridan, T.; Manning, K.W.; Martilli, A.; Miao, S.; et al. The integrated WRF/urban modelling system: Development, evaluation, and applications to urban environmental problems. *Int. J. Climatol.* **2011**, *31*, 273–288. [CrossRef]
6. Chen, F.; Kusaka, H.; Tewari, M.; Bao, J.W.; Hirakuchi, H. Utilizing the coupled WRF/LSM/Urban modeling system with detailed urban classification to simulate the urban heat island phenomena over the Greater Houston area. In Proceedings of the Fifth Symposium on the Urban Environment, Vancouver, BC, Canada, 23–27 August 2004.
7. Yang, B.; Zhang, Y.; Qian, Y. Simulation of urban climate with high-resolution WRF model: A case study in Nanjing, China. *Asia-Pac. J. Atmos. Sci.* **2012**, *48*, 227–241. [CrossRef]
8. Holt, T.; Pullen, J. Urban canopy modeling of the New York City metropolitan area: A comparison and validation of single-and multilayer parameterizations. *Mon. Weather Rev.* **2007**, *135*, 1906–1930. [CrossRef]
9. Meng, W.; Zhang, Y.-X.; Li, J.-N.; Lin, W.-S.; Dai, G.-F.; Li, H.-H. Application of WRF/UCM in the simulation of a heat wave event and urban heat island around Guangzhou. *J. Trop. Meteorol.* **2011**, *17*, 256–265.
10. Grossman-clarke, S.; Zehnder, J.A.; Loridan, T.; Grimmond, C.S.B. Contribution of land use changes to near-surface air temperatures during recent summer extreme heat events in the Phoenix metropolitan area. *J. Appl. Meteorol. Climatol.* **2010**, *49*, 1649–1664. [CrossRef]
11. Jiang, X.; Wiedinmyer, C.; Chen, F.; Yang, Z.-L.; Lo, J.C.-F. Predicted impacts of climate and land use change on surface ozone in the Houston, Texas, area. *J. Geophys. Res. Atmos. (1984–2012)* **2008**. [CrossRef]
12. Chen, J.; Li, Q.; Niu, J.; Sun, L. Regional climate change and local urbanization effects on weather variables in Southeast China. *Stochast. Environ. Res. Risk Assess.* **2011**, *25*, 555–565. [CrossRef]
13. Xiao, D.; Chen, J.; Chen, Z.; Zhang, B. Effect Simulation of Chengdu Fine Underlying Surface Information on Urban Meteorology. *Meteorol. Mon.* **2011**, *37*, 298–308.
14. Kuang, W.; Liu, J.; Zhang, Z.; Lu, D.; Xiang, B. Spatiotemporal dynamics of impervious surface areas across China during the early 21st century. *Chin. Sci. Bull.* **2013**, *58*, 1691–1701. [CrossRef]
15. Miao, S.; Chen, F.; Lemone, M.A.; Tewari, M.; Li, Q.; Wang, Y. An Observational and Modeling Study of Characteristics of Urban Heat Island and Boundary Layer Structures in Beijing. *J. Appl. Meteorol. Climatol.* **2009**. [CrossRef]

16. Lin, C.-Y.; Chen, W.-C.; Chang, P.-L.; Sheng, Y.-F. Impact of the urban heat island effect on precipitation over a complex geographic environment in Northern Taiwan. *J. Appl. Meteorol. Climatol.* **2011**, *50*, 339–353. [CrossRef]
17. Cheng, F.-Y.; Hsu, Y.-C.; Lin, P.-L.; Lin, T.H. Investigation of the effects of different land use and land cover patterns on mesoscale meteorological simulations in the Taiwan area. *J. Appl. Meteorol. Climatol.* **2013**, *52*, 570–587. [CrossRef]
18. Li, Y.; Okaze, T.; Mochida, A. Prediction of the impacts of urbanization using a new assessment system combining an urban expansion model and WRF-Case study for Guangzhou in China. *J. Heat Island Inst. Int.* **2014**, *9*, 133–137.
19. Chen, F.; Yang, X.; Zhu, W. WRF simulations of urban heat island under hot-weather synoptic conditions: The case study of Hangzhou City, China. *Atmos. Res.* **2014**, *138*, 364–377. [CrossRef]
20. Li, Y.; Song, Y.H.; Mochida, A.; Okaze, T. WRF Environment Assessment in Guangzhou City with an Extracted Land-use Map from the Remote Sensing Data in 2000 as an Example. *J. Harbin Inst. Technol.* **2014**, *21*, 26–32.
21. Cheng, C.K.M.; Chan, J.C.L. Impacts of land use changes and synoptic forcing on the seasonal climate over the Pearl River Delta of China. *Atmos. Res.* **2012**, *60*, 25–36. [CrossRef]
22. Kusaka, H.; Kimura, F. Thermal effects of urban canyon structure on the nocturnal heat island: Numerical experiment using a mesoscale model coupled with an urban canopy model. *J. Appl. Meteorol.* **2004**, *43*, 1899–1910. [CrossRef]
23. AL-Ahmadi, F.S.; Hames, A.S. Comparison of Four Classification Methods to Extract Land Use and Land Cover from Raw Satellite Images for Some Remote Arid Areas, Kingdom of Saudi Arabia. *King Abdul. Univ.* **2009**, *20*, 167–191. [CrossRef]
24. Lu, D.; Tian, H.; Zhou, G.; Ge, H. Regional mapping of human settlements in southeastern China with multisensor remotely sensed data. *Remote Sens. Environ.* **2008**, *112*, 3668–3679. [CrossRef]
25. Elvidge, C.D.; Baugh, K.E.; Kihn, E.A.; Kroehl, H.W.; Davis, E.R. Mapping city lights with nighttime data from the DMSP Operational Linescan System. *Photogramm. Eng. Remote Sens.* **1997**, *63*, 727–734.
26. Elvidge, C.D.; Baugh, K.E.; Dietz, J.B.; Bland, T.; Sutton, P.C.; Kroehl, H.W. Radiance Calibration of DMSP-OLS Low-Light Imaging Data of Human Settlements. *Remote Sens. Environ.* **1999**, *68*, 77–88. [CrossRef]
27. Maisongrande, P.; Duchemin, B.; Dedieu, G. VEGETATION/SPOT: An operational mission for the Earth monitoring; presentation of new standard products. *Int. J. Remote Sens.* **2004**, *25*, 9–14. [CrossRef]
28. Willmott, C.J. Some comments on the evaluation of model performance. *Bull. Am. Meteorol. Soc.* **1982**, *63*, 1309–1313. [CrossRef]
29. Srunnaa, M.; Sethuraman, S. A statistical evaluation and comparison of coast point source dispersion models. *Atmos. Environ.* **1986**, *20*, 301–315.
30. Oke, T.R. The energetic basis of the urban heat island. *Quart. J. Royal Meteorol. Soc.* **1982**, *108*, 1–24. [CrossRef]